Results in Physics 5 (2015) 199–205

Contents lists available at ScienceDirect

Results in Physics

journal homepage: www.journals.elsevier.com/results-in-physics

Optimal solution of nonlinear heat and mass transfer in a two-layer flow with nano-Eyring–Powell fluid

Najeeb Alam Khan [a,*], Faqiha Sultan [b], Qammar Rubbab [c]

[a] Department of Mathematical Sciences, University of Karachi, Karachi 75270, Pakistan
[b] Department of Sciences and Humanities, National University of Computer and Emerging Sciences, Karachi 75030, Pakistan
[c] Department of Mathematics, Air University, Multan Campus, Pakistan

ARTICLE INFO

Article history:
Received 25 June 2015
Accepted 18 August 2015
Available online 28 August 2015

Keywords:
Nano-Eyring–Powell
Brownian motion
Two-layer
Thermophoresis

ABSTRACT

This paper deals with the fully-developed two-layer Eyring–Powell fluid in a vertical channel divided into two equal regions. One region is filled with the clear Eyring–Powell fluid and other with the nano-Eyring–Powell fluid. The flow is observed under the uniform wall temperature and concentration boundary conditions for combined heat and mass transfer. The governing coupled nonlinear ordinary differential equations (ODEs) of the flow in each layer are analytically solved by using optimal homotopy analysis method (OHAM) based on the homotopy analysis method (HAM). HAM is an efficient analytical approximation method to solve highly nonlinear problems. The effect of Brownian motion parameter on Eyring–Powell fluid is also observed and the influence of significant parameters is presented for their different values.

1. Introduction

The study of mixed, free and forced convective heat transfer in a vertical parallel plate channel has always gained massive attention because of its wide range applications in many industrial processes. Methodologies to suppress or eliminate interfacial instabilities and further stabilize multi-layer flows, are therefore inherently of interest. Some examples comprise microelectronic cooling, design of cooling system in electronic devices, nuclear reactors cooled during emergency shutdown, chemical processing equipment, solar technology, etc. Initially, Tao [1] has investigated the laminar fully developed mixed convection in a vertical channel and later, this work of Tao was extended by Habchi and Acharya [2] to asymmetric heating where one plate is heated and the other plate is adiabatic. Further, in a vertical channel with asymmetric wall temperature, Aung and Worku [3] analyzed developing flow and flow reversal and then they provided results for mixed convection flow with different wall temperatures [4]. Single-fluid model was considered in all the above mentioned studies, but a large amount of the scientific and technological problems related to plasma physics, petroleum industry, magnetofluid dynamics, geophysics, etc., involve multifluid flow situations. Multilayer flows mainly occur in three different patterns. First of all in co-extrusion processes which make a product of more than one layer concurrently. Secondly, several film coating processes involve a multi-layer, where on each fluid substrate a different layer is used. Thirdly, in lubricated transport processes in which between the walls of a duct and the transported fluid, a lubricating fluid lies in a layer. The flow and the heat transfer of two immiscible fluids were investigated by Nikodijevic et al. [5] in the presence of a uniform inclined magnetic field. And a three-layer unsteady flow in which porous media are sandwiched between viscous fluids was studied by Umavathi et al. [6]. Recently, Farooq et al. investigated the two-layer flow with nanofluids for third grade-fluids [7]. They have considered the mixed-convection in a vertical channel and the fluid properties at the interface are also observed.

The study of nanofluids has now become a global research area and it has gained the massive attention of researchers in the last few years. Its properties are known to be effective on heat transfer and convective flows such as viscosity and thermal conductivity. Water, oil and ethylene glycol mixture are the conventional heat transfer fluids and these fluids are poor at heat transfer. An innovative technique has been used extensively to improve the heat transfer by using ultra fine solid particles in the fluids during the last decade. For this purpose, Choi [8] introduced the term nanofluid which refers to the fluids by suspending nano-scale (less than 1%) particles in the base fluid which increases the thermal conductivity of the fluid up to approximately two times. Nanotechnology is regarded as one of the most significant forces that is the foundation of the next major industrial revolution of this century and it causes many applications in space crafts, electronic devices, artificial organs, metrology and cooling applications of nanofluids,

* Corresponding author.

http://dx.doi.org/10.1016/j.rinp.2015.08.006
2211-3797/

etc. Therefore, nanofluids promise to fetch about a revolution in cooling technologies. As a consequence of these discoveries, research and development on nanofluids has drawn considerable attention from industry and academia over the past several years. For the first time Khanafer et al. [9] examined heat transfer performance of nanofluids enclosing the solid particle dispersion. A detailed review on nanofluids has been given in a book entitled Nanofluids: Science and Technology by Das et al. [10]. For a fully developed flow the effect of nanoparticle volume fraction on velocity and temperature distribution was studied by Xu and Pop [11]. They have also counted into the laminar mixed convection flow of a nanofluid caused by both the buoyancy force and external pressure gradient in a vertical channel [12]. Nadeem et al. [13] inspected the non-aligned stagnation point nano fluid over a convective surface in the presence of a partial slip. Furthermore, they numerically investigated the effect of the magnetic field on the oblique flow of a Walter-B type nano fluid over a convective surface [14].

Eyring–Powell fluid model [15] a complete mathematical model was proposed by Powell and Eyring in 1944. It possesses many advantages over the non-Newtonian fluid models such as it is evoked from the kinetic theory of liquids rather than the empirical relation and also for low and high shear rates it correctly reduces to Newtonian behavior. The flow of an Eyring–Powell model fluid due to a stretching cylinder with variable viscosity under boundary layer conditions was presented by Malik et al. [16]. Hayat et al. [17] examined the steady flow of an Eyring–Powell fluid over a striking surface with convective boundary conditions. Ara et al. [18] investigated the effect of thermal radiations on this flow over an exponentially shrinking sheet.

To the best of authors' knowledge, the non-Newtonian clear Eyring–Powell fluid and non-Newtonian nano-Eyring–Powell fluid has never been investigated together in a two layer vertical channel. This study investigates the steady fully-developed mixed convection flow in a vertical channel and the governing fluid equations in each layer of the channel are more complicated because of the presence of non-Newtonian Eyring–Powell fluid. Buoyancy force using the mathematical nano-fluid model presented by Buongiorno [19], and an outer pressure gradient is used to drive the flow. Until now, many studies have been presented which discuss the influence of different fluid parameters on Eyring–Powell fluid so, this study explicitly focuses on the effects of Brownian motion parameter, buoyancy parameter, and thermophoretic effects on this fluid and it may be considered as the extension of the problem of a two-layer flow of viscous fluid along with viscous nano-fluid investigated by Farooq and Liang [20].

In this paper, the optimal analysis homotopy method (OHAM) via Mathematica package BVPH2.0 is used to solve the governing nonlinear coupled ODEs of the non-Newtonian fluid in both layers. Residual errors and convergence control parameters for different orders of approximation are presented in the tables. Graphical results are displayed to show the influence of several interesting parameters on the fluid flow, heat, and mass transfer. Fluid behavior at the interface is also noted and discussed through the tables. A comparison between the values of the physical properties of the viscous fluid and a special case of Eyring–Powell fluid is presented through the tables.

2. Mathematical model

Mathematically the Eyring–Powell model is presented as

$$A = -pI + \Gamma \tag{1}$$

where extra stress tensor Γ is given by

$$\Gamma = \mu A_1 + \frac{1}{b\dot{\gamma}} \sin h^{-1}\left(\frac{1}{c}\dot{\gamma}\right) A_1 \tag{2}$$

here μ, b and c are the rheological parameters of the Eyring–Powell fluid model [21], μ is the coefficient of shear viscosity and c has the dimension of $(time)^{-1}$. We take the second order approximation of the $(\sin h)^{-1}$ function as

$$\sin h^{-1}\left(\frac{1}{c}\dot{\gamma}\right) \cong \frac{1}{c}\dot{\gamma} - \frac{1}{6}\left(\frac{1}{c}\dot{\gamma}\right)^3, \quad \left|\frac{1}{c}\dot{\gamma}\right| << 1 \tag{3}$$

and Eq. (2) takes the form

$$\Gamma = \left(\mu + \frac{1}{bc}\right) A_1 - \frac{1}{6bc^3}\dot{\gamma}^2 A_1 \tag{4}$$

where $\dot{\gamma} = \sqrt{\frac{1}{2} tr A_1^2}$ and the kinematical tensor A_1 is defined as $A_1 = \nabla V + (\nabla V)^T$.

2.1. Problem formulation

Consider a two-layer vertical channel as shown in Fig. 1, also consider a steady, laminar, boundary layer, and incompressible flow between two vertical parallel plates extended in the x and z direction. l is the width of each layer and the region in the domain $0 \leqslant y \leqslant l$ is filled with clear Eyring–Powell fluid with viscosity μ_1 and density ρ_1. The other region in the domain $-l \leqslant y \leqslant 0$ is filled with nano-Eyring–Powell fluid with viscosity μ_2 and density ρ_2. It is assumed that the pressure gradient is constant in both the regions, but the wall temperature is different for both the boundary walls of the channel. The left wall is held at temperature T_{w2} and the right wall is held at T_{w1} temperature with $T_{w1} > T_{w2}$.

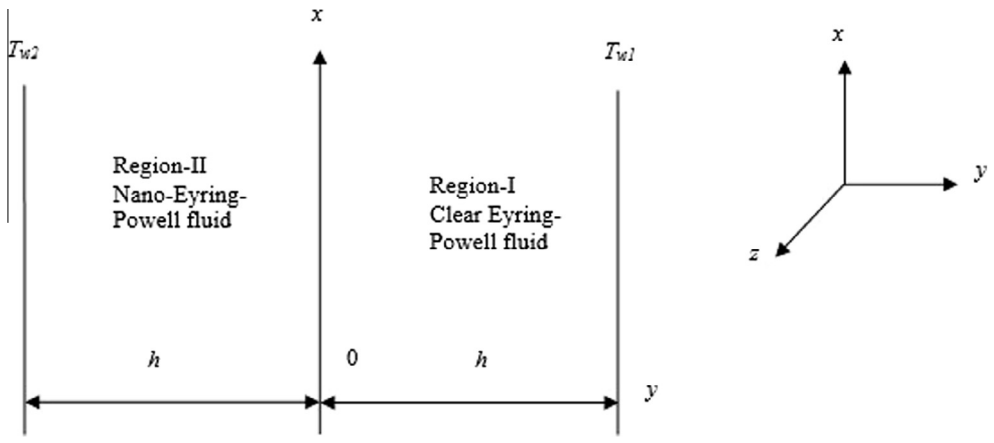

Fig. 1. Physical configuration of the problem.

Under the above assumptions, the governing equations of momentum and energy for the region-I are as follows:

$$\left(\nu_1+\frac{1}{\rho_1 bc}\right)\frac{d^2u_1}{dy^2}-\frac{1}{2\rho_1 bc^3}\left(\frac{du_1}{dy}\right)^2\left(\frac{d^2u_1}{dy^2}\right)-\frac{1}{\rho_1}\frac{\partial p}{\partial x}+g\beta_1(T_1-T_{w2})=0 \tag{5}$$

$$\alpha_1\frac{d^2T_1}{dy^2}+\frac{1}{\rho_1 C_p}\left(\left(\nu_1+\frac{1}{\rho_1 bc}\right)\left(\frac{du_1}{dy}\right)^2-\frac{1}{6\rho_1 bc^3}\left(\frac{du_1}{dy}\right)^4\right)+\frac{Q_1}{\rho_1 C_p}(T_1-T_{w2})=0 \tag{6}$$

and the governing equations of momentum, energy, and nanoparticle volume fraction for region-II are defined as:

$$\left(\nu_2+\frac{1}{\rho_2 bc}\right)\frac{d^2u_2}{dy^2}-\frac{1}{2\rho_2 bc^3}\left(\frac{du_2}{dy}\right)^2\left(\frac{d^2u_2}{dy^2}\right)-\frac{1}{\rho_2}\frac{\partial p}{\partial x}+g\beta_2(T_2-T_{w2})=0 \tag{7}$$

$$\begin{aligned}&\alpha_2\tfrac{d^2T_2}{dy^2}+\tfrac{1}{\rho_2 C_p}\left(\left(\nu_2+\tfrac{1}{\rho_2 bc}\right)\left(\tfrac{du_2}{dy}\right)^2-\tfrac{1}{6\rho_2 bc^3}\left(\tfrac{du_2}{dy}\right)^4\right)\\&+\tau\left(D_B\tfrac{dC}{dy}\tfrac{dT_2}{dy}\left(\tfrac{dT_2}{dy}\right)^2+\tfrac{D_T}{T_{w2}}\left(\tfrac{dT_2}{dy}\right)^2\right)+\tfrac{Q_2}{\rho_2 C_p}(T_2-T_{w2})=0\end{aligned} \tag{8}$$

$$D_B\frac{d^2C}{dy^2}+\frac{D_T}{T_{w2}}\frac{d^2T_2}{dy^2}=0 \tag{9}$$

here the subscripts $i=1,2$ indicate the values for region-I and region-II, respectively. u_i and ν_i are the x and y-components of the velocity vector, ν_i are the kinematic viscosities, Q_i are the absorption parameters or internal heat generations, T_i are the temperatures, g is the gravitational acceleration, β_i are the thermal expansion coefficients, C is the nanoparticle volume fraction, D_T is the coefficient of thermophoretic diffusion, D_B is the coefficient of Brownian diffusion and τ is the heat capacity ratio defined as $\tau=\frac{(\rho C_p)_p}{(\rho C_p)_f}$ with $(\rho C_p)_p$ being heat capacity of the nanoparticle and $(\rho C_p)_f$ being the heat capacity of the base fluid.

The velocity, temperature, shear stress, and the heat flux are supposed to be continuous at the interface [20]. The x-component of the velocity vanishes for no-slip boundary conditions at the interface and there exist isothermal boundary conditions at the temperature. All the above assumptions lead us to the following boundary conditions:

$$\begin{aligned}&u_1(y)=0,\quad T_1(y)=T_{w1}\ \text{at}\ \ y=l,\\&\left.\begin{aligned}&u_1(y)=u_2(y),\quad T_1(y)=T_2(y),\quad C(y)=0\\&\left(\mu_1+\tfrac{1}{bc}\right)\tfrac{du_1}{dy}-\tfrac{1}{6bc^3}\left(\tfrac{du_1}{dy}\right)^3=\left(\mu_2+\tfrac{1}{bc}\right)\tfrac{du_2}{dy}-\tfrac{1}{6bc^3}\left(\tfrac{du_2}{dy}\right)^3,\\&K_1\tfrac{dT_1}{dy}=K_2\tfrac{dT_2}{dy},\end{aligned}\right\}\ \text{at}\ \ y=0,\\&u_2(y)=0,\quad T_2(y)=T_{w2},\quad C(y)=C_w\ \text{at}\ \ y=-l\end{aligned} \tag{10}$$

here K_i represent the thermal conductivities of regions I and II.

2.2. Non-dimensionalization

The fundamental dimensionless quantities are defined as:

$$\begin{aligned}&y^*=\frac{y}{l},\ \ u_i^*=\frac{u_i}{\tilde{u}_i},\ \ T_i=T_{w2}+(T_{w1}-T_{w2})\theta_i(y),\ \ C=C_w\phi(y),\\&P_i=-\frac{l^2}{\mu_i\tilde{u}_i}\frac{\partial p}{\partial x},\ \ Gr_i=\frac{g\beta_i(T_{w1}-T_{w2})l^3}{\nu_i^2},\ \ \mathrm{Re}_i=\frac{\tilde{u}_i l}{\nu_i}\end{aligned} \tag{11}$$

here $\tilde{u}_i$ symbolize the average velocities in regions I and II. Substituting the above defined non-dimensional similarity variables in Eqs. (5)–(9) give us the following non-dimensional governing equations:

Region-I

$$(1+M_1)\frac{d^2u_1}{dy^2}-M_1\gamma_1\left(\frac{du_1}{dy}\right)^2\frac{d^2u_1}{dy^2}+P_1+\lambda_1\theta_1=0 \tag{12}$$

$$\frac{1}{\mathrm{Pr}_1}\frac{d^2\theta_1}{dy^2}+Ec\left((1+M_1)\left(\frac{du_1}{dy}\right)^2-\frac{M_1\gamma_1}{3}\left(\frac{du_1}{dy}\right)^4\right)+\delta_1\theta_1=0 \tag{13}$$

Region-II

$$(1+M_2)\frac{d^2u_2}{dy^2}-M_2\gamma_2\left(\frac{du_2}{dy}\right)^2\frac{d^2u_2}{dy^2}+P_2+\lambda_2\theta_2=0 \tag{14}$$

$$\begin{aligned}&\frac{1}{\mathrm{Pr}_2}\frac{d^2\theta_2}{dy^2}+Ec\left((1+M_2)\left(\frac{du_2}{dy}\right)^2-\frac{M_2\gamma_2}{3}\left(\frac{du_2}{dy}\right)^4\right)\\&+N_b\frac{d\theta_2}{dy}\frac{d\phi}{dy}+N_t\left(\frac{d\theta_2}{dy}\right)^2+\delta_2\theta_2=0\end{aligned} \tag{15}$$

$$\frac{d^2\phi}{dy^2}+\frac{N_t}{N_b}\frac{d^2\theta_2}{dy^2}=0 \tag{16}$$

P_1 and P_2 are the unknown pressure constants in Eqs. (12) and (14), therefore, conveniently, we differentiate these two equations with respect to y to get equations independent of these pressure constants.

$$(1+M_1)\frac{d^3u_1}{dy^3}-M_1\gamma_1\left(2\frac{du_1}{dy}\left(\frac{d^2u_1}{dy^2}\right)^2+\left(\frac{du_1}{dy}\right)^2\frac{d^3u_1}{dy^3}\right)+\lambda_1\frac{d\theta_1}{dy}=0 \tag{17}$$

$$(1+M_2)\frac{d^3u_2}{dy^3}-M_2\gamma_2\left(2\frac{du_2}{dy}\left(\frac{d^2u_2}{dy^2}\right)^2+\left(\frac{du_2}{dy}\right)^2\frac{d^3u_2}{dy^3}\right)+\lambda_2\frac{d\theta_2}{dy}=0 \tag{18}$$

in Eqs. (12)–(18), $M_i=\frac{1}{\mu_i bc}$ and $\gamma_i=\frac{\tilde{u}_i^2}{2c^2l^2}$ are the rheological parameters, $\lambda_i=\frac{Gr_i}{\mathrm{Re}_i}$ are the mixed convection parameters, $\mathrm{Pr}_i=\frac{\nu_i}{\alpha_i}$ are the Prandtl numbers and $\delta_i=\frac{Q_i l^2}{\rho_i C_p \nu_i}$ are the heat source/sink parameters in region-I and region-II, respectively, $N_b=\frac{\tau D_B C_w}{\nu_2}$ is the Brownian motion parameter and $N_t=\frac{\tau D_T(T_{w1}-T_{w2})}{\nu_2 T_{w2}}$ is the thermophoretic parameter in region-II containing nano-Eyring–Powell fluid.

The corresponding boundary conditions in Eq. (10) are defined in dimensionless form as:

$$\begin{aligned}&u_1(y)=0,\ \ \theta_1(y)=1\ \text{at}\ y=1,\\&\left.\begin{aligned}&u_1(y)=u_2(y),\ \ \theta_1(y)=\theta_2(y),\ \ \phi(y)=0,\\&(1+M_1)\tfrac{du_1}{dy}-\tfrac{M_1\gamma_1}{3}\left(\tfrac{du_1}{dy}\right)^3=\tfrac{1}{\mu}\left((1+M_2)\tfrac{du_2}{dy}-\tfrac{M_2\gamma_2}{3}\left(\tfrac{du_2}{dy}\right)^3\right),\\&\tfrac{d\theta_1}{dy}=\tfrac{1}{K}\tfrac{d\theta_2}{dy},\end{aligned}\right\}\ \text{at}\ y=0,\\&u_2(y)=0,\ \ \theta_2(y)=0,\ \ \phi(y)=1\text{at}\ y=-1\end{aligned} \tag{19}$$

where $\mu=\frac{\mu_1}{\mu_2}$ and $K=\frac{K_1}{K_2}$.

The mass flux conservation relations at two different cross sections in the channel are considered as the boundary conditions and are given as:

$$\int_0^1 u_1(y)dy = \int_{-1}^0 u_2(y)dy = 1 \tag{20}$$

The most significant physical quantities of practical and engineering interests are the local skin friction coefficient C_f , the local Nusselt number N_u and the local Sherwood number S_h are defined as

$$(C_f, N_u, S_h) = \left(\frac{\Gamma_w}{\rho_i \tilde{u}_i^2}, \frac{x q_w}{K_i(T_{w1} - T_{w2})}, \frac{x M_w}{D_B C_w}\right)\Big|_{y=-1,\,0,\,1} \tag{21}$$

where the local wall shear stress Γ_w, local surface heat flux q_w and the local mass flux M_w are given from the following definitions

$$(\Gamma_w, q_w, M_w) = \left(\left(\nu_i + \frac{1}{\rho_i bc}\right)\frac{du_i}{dy} - \frac{1}{2\rho_i bc^3}\left(\frac{du_i}{dy}\right)^3, -K_i\frac{dT_i}{dy}, -D_B\frac{dC}{dy}\right)\Big|_{y=-1,\,0,\,1} \tag{22}$$

using above definitions in Eq. (21) give the local skin friction coefficient C_f , the local Nusselt number N_u and the local Sherwood number S_h as:

$$\left(\mathrm{Re}_x^{\frac{1}{2}} C_f, \mathrm{Re}_x^{-\frac{1}{2}} N_u, \mathrm{Re}_x^{-\frac{1}{2}} S_h\right) = \left((1+M_i)\frac{du_i}{dy} - \frac{M_i\gamma_i}{3}\left(\frac{du_i}{dy}\right)^3\Big|_{y=-1,0,1}, -\frac{d\theta_i}{dy}\Big|_{y=-1,0,1}, -\frac{d\phi_i}{dy}\Big|_{y=0,1}\right) \tag{23}$$

where $\mathrm{Re}_i = \frac{\tilde{u}_i l}{\nu_i}$ are the local Reynolds numbers.

3. Analytical approximation by means of HAM

The homotopy analysis method (HAM) first presented by Liao [22,23] is used to obtain the analytical solutions. HAM is very powerful to find analytical solutions as it provides huge flexibility to choose the convergence region with the help of the convergence control parameter $\hbar$ and several interesting problems have been solved by this method [24–26]. An efficient analytical optimal homotopy analysis method (OHAM) by BVPh2.0 Mathematica package will also be used to calculate some optimal solutions, the residual errors and convergence control parameters of the series solutions. OHAM based on HAM was proposed by Liao [27] and is an efficient analytic tool to solve ordinary differential equations and even some partial differential equations.

We select the auxiliary linear operators, $L_1[u_i], L_2[(\theta_i, \phi)]$ as

$$(L_1[u_i], L_2[(\theta_i, \phi)]) = \left(\frac{d^3u_i}{dy^3}, \frac{d^2(\theta_i, \phi)}{dy^2}\right) \tag{24}$$

The auxiliary linear operators defined in Eq. (24) satisfy the following properties

$$(L_1[u_i], L_2[(\theta_i, \phi)]) = (L_1[c_1y^2 + c_2y + c_3], L_2[c_4y + c_5]) = 0 \tag{25}$$

where $c_1, c_2, \ldots, c_5$ are the constants to be determined.

HAM gives us the freedom to choose the initial guess. All the initial guesses must satisfy the boundary conditions and the two supplementary constraints defined in Eqs. (15) and (17)–(20). We chose the initial approximations satisfying the above mentioned conditions as:

$$(u_{i,0}(y), \theta_{1,0}(y), \theta_{2,0}(y), \phi_0(y)) = \left(\frac{3}{2}(1-y^2), \frac{1}{K}y + \left(1 - \frac{1}{K}\right)y^2, y + y^2, \frac{1}{2}y + \frac{3}{2}y^2\right) \tag{26}$$

4. Optimal convergence-control parameters

It is noted that in HAM the terms $u_{i,m}(y)$, $\theta_{i,m}(y)$ and $\phi_m(y)$ (where m is the order of approximation) contain the unknown convergence-control parameters $\hbar_{u_1}$, $\hbar_{u_2}$, $\hbar_{\theta_1}$, $\hbar_{\theta_2}$ and $\hbar_\phi$ which determine the convergence region and rate of the homotopy-series solutions. To determine the optimal values of these parameters we use the so called average squared residual error defined by Liao [22,23].

$$E_m^{u_1}(y) = \frac{1}{r+1}\sum_{j=0}^{r}\left[N_1\left(\sum_{i=0}^{m}u_{1,i}(y), \sum_{i=0}^{m}\theta_{1,i}(y)\right)_{y=j\Delta y}\right]^2 dy, \tag{27}$$

$$E_m^{u_2}(y) = \frac{1}{r+1}\sum_{j=0}^{r}\left[N_2\left(\sum_{i=0}^{m}u_{2,i}(y), \sum_{i=0}^{m}\theta_{2,i}(y)\right)_{y=-1+j\Delta y}\right]^2 dy, \tag{28}$$

$$E_m^{\theta_1}(y) = \frac{1}{r+1}\sum_{j=0}^{r}\left[N_3\left(\sum_{i=0}^{m}u_{1,i}(y), \sum_{i=0}^{m}\theta_{1,i}(y)\right)_{y=j\Delta y}\right]^2 dy, \tag{29}$$

$$E_m^{\theta_2}(y) = \frac{1}{r+1}\sum_{j=0}^{r}\left[N_4\left(\sum_{i=0}^{m}u_{2,i}(y), \sum_{i=0}^{m}\theta_{2,i}(y), \sum_{i=0}^{m}\phi_i(y)\right)_{y=-1+j\Delta y}\right]^2 dy, \tag{30}$$

$$E_m^{\phi}(y) = \frac{1}{r+1}\sum_{j=0}^{r}\left[N_5\left(\sum_{i=0}^{m}\phi_i(y), \sum_{i=0}^{m}\theta_{2,i}(y)\right)_{y=-1+j\Delta y}\right]^2 dy, \tag{31}$$

and

$$E_m^t(y) = E_m^{u_1}(y) + E_m^{u_2}(y) + E_m^{\theta_1}(y) + E_m^{\theta_2}(y) + E_m^{\phi} \tag{32}$$

where $E_m^t(y)$ is the total squared residual error, $\Delta y = 0.5$ and $r = 20$.

We have computed the average squared residual errors at 40th order of approximation by using the optimal convergence control parameters corresponding to the 2nd order of approximation for a particular case with $\lambda_1 = \mathrm{Pr}_i = h = 1$, $N_t = 0.01$, $N_b = \delta_i = Ec = \gamma_i = M_i = 0.1$ and $\mu = K = 0.5$. The results obtained from Eqs. (15) and (17)-(20) are substituted in Eqs. (14) and (16) to determine the values of unknown pressure constants P_1 and P_2 at the interface. For the convergence control parameters $(^{-}h_{u_1}, ^{-}h_{u_2}, ^{-}h_{\theta_1}, ^{-}h_{\theta_2}, ^{-}h_\phi) = (-0.956, -1.063, -0.933, -0.928, -0.887)$, the average squared residuals are $(E_m^{u_1}(y), E_m^{u_2}(y), E_m^{\theta_1}(y), E_m^{\theta_2}(y), E_m^{\phi}(y)) = (5.33 \times 10^{-31}, 8.27 \times 10^{-32}, 2.15 \times 10^{-31}, 4.42 \times 10^{-31}, 1.64 \times 10^{-32})$ and the total squared residual error is $E_m^t(y) = 8.53 \times 10^{-31}$ and the pressure constants are $(P_1, P_2) = (578.6, 561.8)$.

Table 1
Numerical values of local skin friction coefficient C_f and the local Nusselt number N_u for physical parameters M_1, N_b, N_t in region-I.

M	N_b	N_t	$\mathrm{Re}^{\frac{1}{2}}C_f\big\|_{y=0}$	$\mathrm{Re}^{\frac{1}{2}}C_f\big\|_{y=1}$	$\mathrm{Re}^{-\frac{1}{2}}N_u\big\|_{y=0}$	$\mathrm{Re}^{-\frac{1}{2}}N_u\big\|_{y=1}$
0.0			0.019	2.982	0.782	2.589
0.2	0.1	0.1	0.024	3.249	0.791	0.144
0.4			0.137	3.309	0.805	0.421
	0.01		0.156	2.310	0.691	2.438
0.2	0.1	0.1	0.224	2.288	0.684	2.207
	0.3		0.262	2.259	0.679	2.194
		0.01	0.156	2.310	0.682	2.388
0.2	0.1	0.1	0.157	2.315	0.823	2.250
		0.3	0.159	2.321	0.999	2.072

Table 2
Numerical values of local skin friction coefficient C_f , local Nusselt number N_u and the local Sherwood S_h number for physical parameters M_2, N_b, N_t in region-II.

M	N_b	N_t	$\mathrm{Re}^{\frac{1}{2}}C_f\big\|_{y=0}$	$\mathrm{Re}^{\frac{1}{2}}C_f\big\|_{y=-1}$	$\mathrm{Re}^{-\frac{1}{2}}N_u\big\|_{y=0}$	$\mathrm{Re}^{-\frac{1}{2}}N_u\big\|_{y=-1}$	$\mathrm{Re}^{-\frac{1}{2}}S_h\big\|_{y=0}$	$\mathrm{Re}^{-\frac{1}{2}}S_h\big\|_{y=-1}$
0.0			0.038	2.946	0.782	3.422	1.798	0.782
0.2	0.1	0.1	0.024	3.222	0.791	0.708	36.01	0.791
0.4			0.080	3.400	0.695	0.269	38.50	0.695
	0.01		0.046	2.377	0.691	3.325	2.982	0.691
0.2	0.1	0.1	0.048	2.304	0.694	3.104	3.249	0.694
	0.3		0.092	2.258	0.679	3.280	2.309	0.679
		0.01	0.046	2.377	0.682	3.263	2.310	0.682
0.2	0.1	0.1	0.043	2.380	0.823	2.695	2.288	0.823
		0.3	0.042	2.384	0.999	2.051	2.259	0.999

Table 3
Comparison between the values of velocity components of viscous fluid and a special case of Eyring–Powell fluid ($M = Ec = 0$) at the interface and right boundary wall of region-I.

N_t	N_b	Viscous fluid		Eyring–Powell fluid ($M = Ec = 0$)	
		$-\frac{du_1}{dy}(0)$	$-\frac{du_1}{dy}(1)$	$-\frac{du_1}{dy}(0)$	$-\frac{du_1}{dy}(1)$
	0.01	10.8294	14.9014	10.8294	14.9015
0.01	0.1	10.7782	14.8107	10.7782	14.8108
	0.3	10.7658	14.8011	10.7658	10.7659
0.1	0.01	10.8283	14.8992	10.8283	14.8992
0.3	0.01	10.8259	14.8943	10.8259	14.8944

Table 4
Comparison between the values of velocity components of the viscous fluid and a special case of Eyring–Powell fluid ($M = Ec = 0$) at the interface and left boundary wall of region-II.

N_t	N_b	Viscous fluid		Eyring–Powell fluid ($M = Ec = 0$)	
		$-\frac{du_1}{dy}(0)$	$-\frac{du_1}{dy}(-1)$	$-\frac{du_1}{dy}(0)$	$-\frac{du_1}{dy}(-1)$
	0.01	5.4147	6.2677	5.4147	6.2677
0.01	0.1	5.3891	6.1780	5.3891	6.1780
	0.3	5.3829	6.1684	5.3829	6.1684
0.1	0.01	5.4141	6.2656	5.4141	6.2656
0.3	0.01	5.4129	6.2611	5.4129	6.2611

5. Results and discussion

This section explains the effects of significant parameters of the fluid and nanoparticle volume fraction on velocity, heat, and mass transfer in two regions of a vertical channel. One region was filled with clear Eyring–Powell fluid and the other with nano-Eyring–Powell fluid. For the conciseness of the study, the fluid parameters in the region-I and region-II are considered as $(\xi_1, \delta_1, M_1, \gamma_1) = (\xi_2, \delta_2, M_2, \gamma_2)$ and for these substantial parameters, magnitude of the numerical values of different physical parameters such as local skin friction coefficients C_f, local Nusselt number N_u and the local Sherwood number S_h are presented in Tables 1 and 2 for region-I and region-II, respectively.

The skin friction is given by $\mathrm{Re}_x^{\frac{1}{2}}C_f$ which is mathematically presented in Eq. (23). Since $\frac{du_i}{dy}$ is negative which is being multiplied by $(1 + M_i)$ greater than 1 and the second term $-(\frac{du_i}{dy})^3$ is positive which is multiplied by a fraction $\frac{M_i\gamma_i}{3}$ less than 1 which makes the magnitude of the skin friction coefficient increase with an increase in M_i. In Tables 1 and 2, with an increase in the parameters $M_i, N_b,$ and N_t , the local skin friction coefficient C_f is observed to be increasing at the interface and the boundary walls but opposite behavior for local Nusselt number N_u and the local Sherwood number S_h is observed. A very slight alteration in these physical quantities is observed with an increase in Eyring–Powell parameters, Brownian motion parameter and thermophoretic parameter in the region-I and II. Tables 3 and 4 present the comparison between the values of velocity components of the viscous fluid and a special case of Eyring–Powell fluid ($M = Ec = 0$) at the interface and the boundary walls of region-I and II keeping $\lambda_1 = 150$, $\mathrm{Pr}_1 = 2$, $\mathrm{Pr}_2 = 7$, $\gamma_i = h = 1$, $M_i = 0.2$, $\delta_i = 0.0$, and $\mu = K = 0.5$. The obtained results show a remarkable agreement which validates the fluid model.

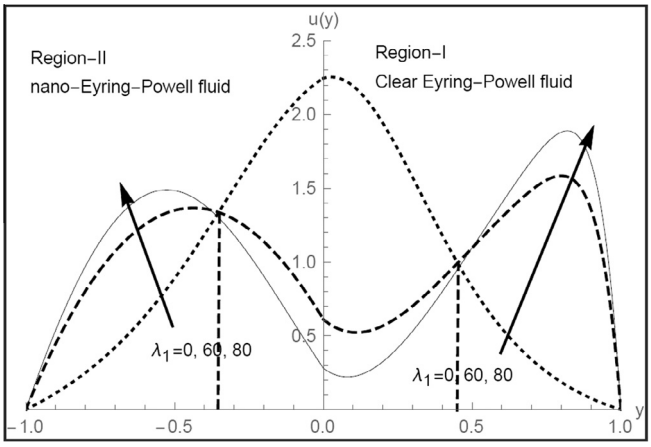

Fig. 2. Influence of buoyancy parameter λ_1 on velocity $u(y)$.

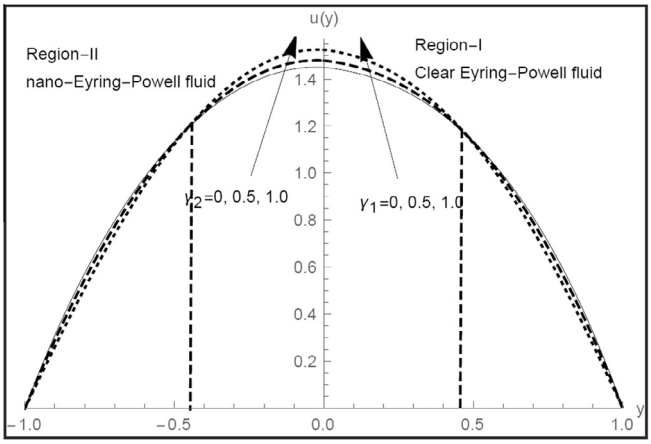

Fig. 3. Influence of non-Newtonian fluid parameter γ_i on velocity $u(y)$.

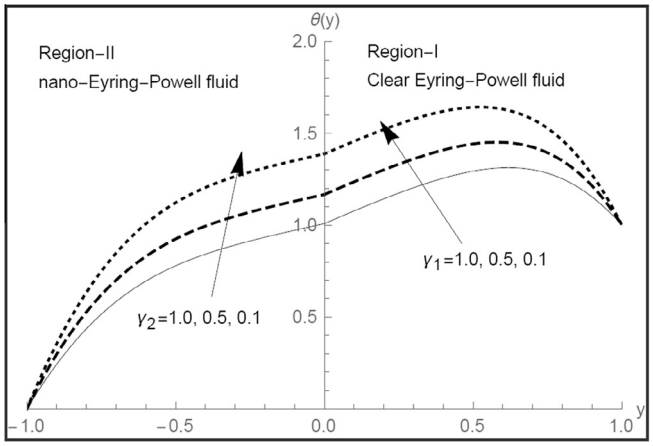

Fig. 4. Behavior of temperature profiles $\theta(y)$ for non-Newtonian fluid parameters γ_i.

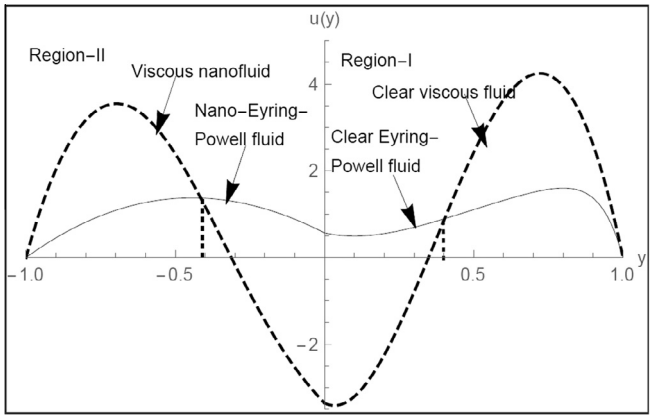

Fig. 5. Influence of Eyring–Powell parameters M_i and velocity $u(y)$ comparison for viscous fluid ($M_i = 0$) and Eyrin–Powell fluid.

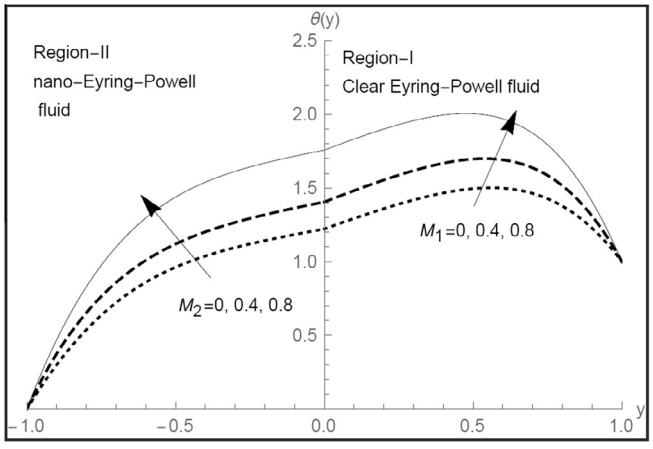

Fig. 6. Behavior of temperature profiles $\theta(y)$ for Eyring–Powell fluid parameter M_i.

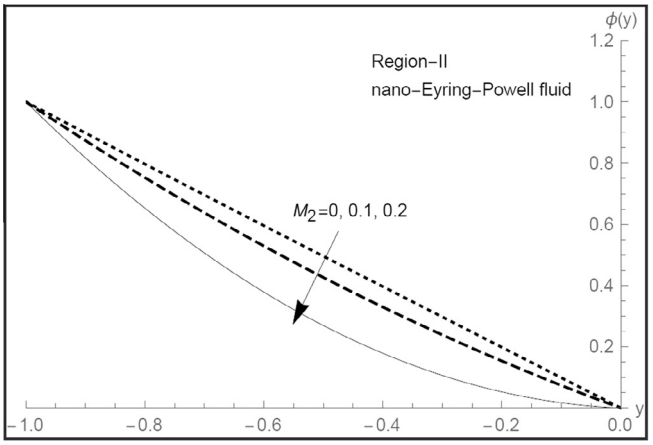

Fig. 7. Behavior of concentration profiles $\phi(y)$ for Eyring–Powell fluid parameter M_2 in region-II.

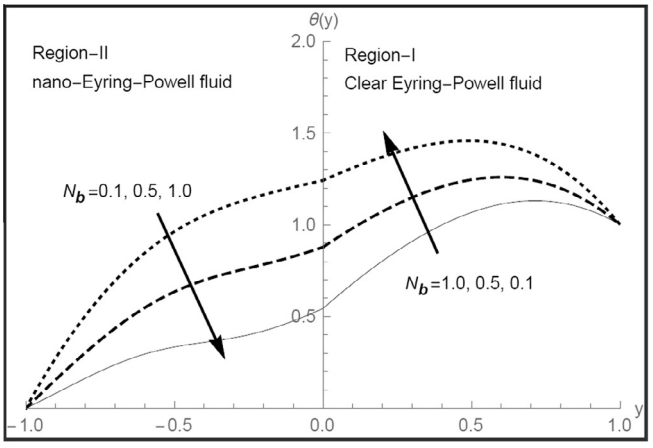

Fig. 8. Behavior of temperature profiles $\theta(y)$ for Brownian parameter N_b.

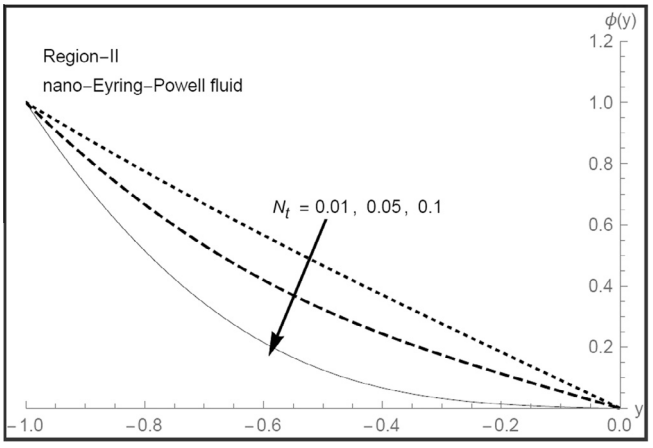

Fig. 9. Behavior of concentration profiles $\phi(y)$ for thermophoretic parameter N_t in region-II.

Figs. 2–10 present the behavior of velocity $u(y)$, temperature profiles $\theta(y)$ and the concentration profiles $\phi(y)$ for different fluid parameters, $\lambda_i = \frac{Gr_i}{Re_i}$ the mixed convection parameters, M_i the Eyring–Powell parameters, γ_i the non-Newtonian parameters, Pr_i the Prandtl numbers, δ_i the heat source/sink parameters, N_b the Brownian motion parameter and N_t the thermophoretic parameter, while keeping $\lambda_1 = 5$, $\gamma_i = Pr_i = 5, h = 1$, $M_i = 0.2$, $N_b = \delta_i = 0.1$, $N_t = 0.01$ and $\mu = K = 0.5$.

Fig. 2 shows the behavior of velocity for mixed convection parameter λ_1, also known as the buoyancy parameter. The velocity profile shows increasing behavior for the forced convection i.e.

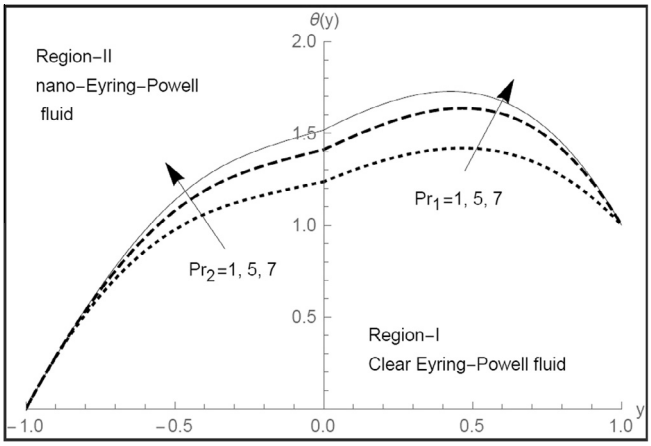

Fig. 10. Behavior of temperature profiles $\theta(y)$ for Prandtl numbers Pr_i.

$\lambda_1 \to 0$ and reaches to its maximum value $u(y) = 2.39$ at the interface. The reversed behavior of the velocity profiles is observed for free convection i.e. $\lambda_1 \to \infty$, the fluid flow reverses its direction for large values of the buoyancy parameter and it changes the direction at $y = 0.45$ in region-I and at $y = -0.45$ in region-II. Figs. 3 and 4 depict the effect of non-Newtonian parameters γ_i on velocity and temperature profiles respectively. Fig. 3 shows that the velocity of the fluid increases in both the regions but decreases at the interface and it is observed in Fig. 4 that the heat transfer decreases as the non-Newtonian parameter increases. Figs. 5–7 illustrate the effect of fluid parameters M_i on velocity, temperature and concentration profiles. For sufficiently large buoyancy parameter $\lambda_1 = 100$, a comparison in velocity profiles of viscous fluid $M_i = 0$ and Eyring–Powell fluid for $M_i = 0.4$ is presented in Fig. 5. Viscous fluid shows high velocity profiles in both the regions and because of the high buoyancy ratio, both the fluids reversed their direction at $y = 0.4$ in region-I and at $y = -0.4$ in region-II. Fig. 6 demonstrates that the increase in M_i increases the heat transfer but opposite behavior for mass transfer is observed in Fig. 7.

In Figs. 8 and 9, the influence of Brownian motion parameter N_b on heat transfer, and thermophoretic parameter N_t on mass transfer is presented respectively, and it is noted that the heat transfer of the fluid is reduced when the Brownian motion is increased and the mass transfer in the fluid is reduced when the thermophoresis is increased. Increase in Prandtl numbers Pr_i increases the heat transfer phenomena in the fluid as depicted in Fig. 10.

6. Conclusion

In this study, the two-layer Eyring–Powell fluid flow in a vertical channel along with nanoparticles, termed as nano-Eyring–Powell fluid has been investigated. The vertical channel was divided into two regions out of which one was filled with clear viscous fluid and other with nano-Eyring–Powell fluid and width of the regions was assumed to be equal. More or less significant and interesting findings of the investigation are listed below

1. Sufficiently large buoyancy parameter or free convection can reverse the flow.
2. Flow changes its direction in the interval $[-0.45, 0.45]$
3. Eyring–Powell parameter reduces the fluid flow, heat and mass transfer.
4. Increase in Brownian motion parameter reduces the heat transfer in the flow.
5. Mass transfer in the fluid reduces as the thermophoretic parameter increases.
6. Increase in Pr_i increases the temperature profiles.
7. Comparison of the results validates the fluid model.

References

[1] Tao LN. On combined free and forced convection in channels. ASME J Heat Transfer 1960;82:233–8.
[2] Habchi S, Acharya S. Laminar mixed convection in a symmetrically or asymmetrically heated vertical channel. Numer Heat Transfer 1986;5:605–18.
[3] Aung W, Worku G. Developing flow and flow reversal in a vertical channel with asymmetric wall temperature. ASME J Heat Transfer 1986;108:299–304.
[4] Aung W, Worku G. Theory of fully developed, combined convection including flow reversal. ASME J Heat Transfer 1986;108:485–8.
[5] Nikodijevic D, Stamenkovic Z, Milenkovic D, Lagojevic B, Nikodikevic J. Flow and heat transfer of two immiscible fluids in the presence of uniform inclined magnetic field. Math Prob Eng 2011:132302.
[6] Umavathi JC, Liu IC, Kumar JP, Meera DS. Unsteady flow and heat transfer of porous media sandwiched between viscous fluids. Appl Math Mech 2010;31:1497–516.
[7] Farooq U, Hayat T, Alsaedi A, Liao SJ. Heat and mass transfer of two-layer flows of third-grade nano-fluids in a vertical channel. Appl Math Comput 2014;242:528–40.
[8] Choi SUS. Enhancing thermal conductivity of fluids with nanoparticle. In: The proceedings of the 1995 ASME international mechanical engineering congress and exposition, San Francisco, USA, ASME, FED 231/MD 66; 1995. p. 99–105.
[9] Khanafer K, Vafai K, Lightstone M. Buoyancy-driven heat transfer enhancement in a two-dimensional enclosure utilizing nanofluids. Int J Heat Mass Transfer 2003;46:3639–53.
[10] Das SK, Choi SUS, Yu WY, Pradeep T. Nanofluid: science and technology. New Jersey: Wiley Interscience; 2007.
[11] Xu H, Pop I. Fully developed mixed convection flow in a vertical channel filled with nanofluids. Int Commun Heat Mass Transfer 2012;39:1086–92.
[12] Fan T, Xu H, Pop I. Mixed convection heat transfer in horizontal channel filled with nanofluids. Appl Math Mech -Engl Ed 2013;34:339–50.
[13] Nadeem S, Mehmood R, Akbar NS. Partial slip effect on non-aligned stagnation point nanofluid over a stretching convective surface. Chin Phys B 2015;24:014702.
[14] Nadeem S, Mehmood R, Motsa SS. Numerical investigation on MHD oblique flow of Walter's B type nano fluid over a convective surface. Int J Therm Sci 2015;92:162–72.
[15] Powell RE, Eyring H. Mechanisms for the relaxation theory of viscosity. Nature 1944;154:427–8.
[16] Malik MY, Hussain A, Nadeem S. Boundary layer flow of an Eyring–Powell model fluid due to a stretching cylinder with variable viscosity. Sci Iranica 2013;20:313–21.
[17] Hayat T, Iqbal Z, Qasim M, Obaidat S. Steady flow of an Eyring Powell fluid over a moving surface with convective boundary conditions. Int J Heat Mass Transfer 2012;55:1817–22.
[18] Ara A, Khan NA, Khan H, Sultan F. Radiation effect on boundary layer flow of an Eyring–Powell fluid over an exponentially shrinking sheet. Ain Shams Eng J. doi:http://dx.doi.org/10.1016/j.asej.2014.06.002.
[19] Buongiorno J. Convective transport in nano fluids. ASME J Heat Transfer 2006;128:240–50.
[20] Farooq U, Liang LZ. Nonlinear heat transfer in a two-layer flow with nanofluids by OHAM. J Heat Transfer 2014;136:021702.
[21] Patel M, Timol MG. Similarity solutions of boundary layer flow of non-Newtonian fluids. Int J Nonlinear Mech 1986;21:475–81.
[22] Liao SJ. The proposed homotopy analysis techniques for the solution of nonlinear problems Ph.D. Dissertation. Shanghai: Shanghai Jiao Tong University; 1992.
[23] Liao SJ. Notes on the homotopy analysis method: Some definitions and theorems. Commun Nonlinear Sci Numur Simul 2009;14:983–97.
[24] Abbasbandy S, Shivanian E. Prediction of multiplicity of solutions of nonlinear boundary value problems: novel application of homotopy analysis method. Commun Nonlinear Sci Numer Simul 2010;15:3830–46.
[25] Khan NA, Jamil M, Khan Nadeem A. Effects of slip factors on unsteady stagnation point flow and heat transfer towards a stretching sheet: an analytical study. Heat Transfer Res 2012;43:779–94.
[26] Hayat T, Qasim M, Abbas Z. MHD flow and mass transfer of a Jeffery fluid over a nonlinear stretching surface. Z Naturforsch A 2009;65:1111–20.
[27] Liao SJ. An optimal homotopy-analysis approach for strongly nonlinear differential equations. Commun Nonlinear Sci Numer Simul 2010;15:2003–16.